work: Variation within a species reflects the range of habitats it inhabits, each with differential importance of the tasks. Thus, populations should be distributed on the same Pareto front as different species facing the same tasks.

Finally, Pareto optimality need not be the only or generic explanation for low dimensionality and lines/triangles in biological data. It may work for some examples and not others, especially if biological constraints other than natural selection are important. The following experimental tests can refute the theory in a specific example: (i) A point in the middle of the front has higher performance in one of the tasks than a point close to the relevant vertex (this might also imply that different tasks are at play). (ii) A mutant can be found that has higher performance at all tasks than existing phenotypes. Both of these tests require measuring performance (*1*, *7*, *13*)— but not the more difficult task of measuring fitness. (iii) Laboratory evolution experiments can follow a mutant that is off the Pareto front (has lower performance in all tasks than the wild type), under conditions in which all tasks are required. Provided with sufficient genetic variation, the mutant is predicted to evolve phenotypes closer to the front.

References and Notes

1. S. J. Arnold, *Am. Zool.* **23**, 347 (1983).
2. G. F. Oster, E. O. Wilson, *Caste and Ecology in the Social Insects* (Princeton Univ. Press, Princeton, NJ, 1979).
3. K. D. Farnsworth, K. J. Niklas, *Funct. Ecol.* **9**, 355 (1995).
4. H. El Samad, M. Khammash, C. Homescu, L. Petzold, Optimal performance of the heat-shock gene regulatory network, *Proc. 16th IFAC World Congress* (2005).
5. M. C. Kennedy, *Ecol. Res.* **25**, 723 (2010).
6. R. E. Steuer, *Multiple Criteria Optimization: Theory, Computation, and Application* (Wiley, New York, 1986).
7. G. R. McGhee, *The Geometry of Evolution: Adaptive Landscapes and Theoretical Morphospaces* (Cambridge Univ. Press, Cambridge, 2007).
8. Supplementary materials are available on *Science* Online.
9. S. J. Gould, *Biol. Rev. Camb. Philos. Soc.* **41**, 587 (1966).
10. C. P. Klingenberg, *Nat. Rev. Genet.* **11**, 623 (2010).
11. K. D. Kavanagh, A. R. Evans, J. Jernvall, *Nature* **449**, 427 (2007).
12. G. B. West, J. H. Brown, B. J. Enquist, *Science* **276**, 122 (1997).
13. P. R. Grant, I. Abbott, D. Schluter, R. L. Curry, L. K. Abbott, *Biol. J. Linn. Soc. Lond.* **25**, 1 (1985).
14. Software that analyzes data in terms of triangles and their significance, and suggests archetype trait values, is available at www.weizmann.ac.il/mcb/UriAlon.
15. E. O. Wilson, *Behav. Ecol. Sociobiol.* **7**, 143 (1980).
16. U. M. Norberg, J. M. V. Rayner, *Philos. Trans. R. Soc. Lond. B Biol. Sci.* **316**, 335 (1987).
17. T. Nyström, *Mol. Microbiol.* **54**, 855 (2004).
18. A. Zaslaver *et al.*, *PLOS Comput. Biol.* **5**, e1000545 (2009).
19. M. Scott, C. W. Gunderson, E. M. Mateescu, Z. Zhang, T. Hwa, *Science* **330**, 1099 (2010).
20. N. Geva-Zatorsky *et al.*, *Cell* **140**, 643 (2010).
21. D. Schluter, *Evolution* **50**, 1766 (1996).

Acknowledgments: We thank N. Barkai, R. Milo, O. Feinerman, C. Tabin, J. Losos, M. Khammash, T. Dayan, and N. Ulanovski for discussion. U.A. holds the Abisch-Frenkel Professorial Chair; O.S. is an Azrieli Fellow. This work was supported by the Israel Science Foundation and the European Research Council (FP7).

Supplementary Materials

www.sciencemag.org/cgi/content/full/science.1217405/DC1
Materials and Methods
Figs. S1 to S24
Table S1
References (*22*–*46*)

2 December 2011; accepted 6 April 2012
Published online 26 April 2012;
10.1126/science.1217405

Chitin-Induced Dimerization Activates a Plant Immune Receptor

Tingting Liu,[1,2,3,4]* Zixu Liu,[4,5]* Chuanjun Song,[6] Yunfei Hu,[7,8] Zhifu Han,[2,3] Ji She,[8] Fangfang Fan,[6] Jiawei Wang,[3] Changwen Jin,[7,8] Junbiao Chang,[6]† Jian-Min Zhou,[4,9]† Jijie Chai[2,3]†

Pattern recognition receptors confer plant resistance to pathogen infection by recognizing the conserved pathogen-associated molecular patterns. The cell surface receptor chitin elicitor receptor kinase 1 of *Arabidopsis* (AtCERK1) directly binds chitin through its lysine motif (LysM)–containing ectodomain (AtCERK1-ECD) to activate immune responses. The crystal structure that we solved of an AtCERK1-ECD complexed with a chitin pentamer reveals that their interaction is primarily mediated by a LysM and three chitin residues. By acting as a bivalent ligand, a chitin octamer induces AtCERK1-ECD dimerization that is inhibited by shorter chitin oligomers. A mutation attenuating chitin-induced AtCERK1-ECD dimerization or formation of nonproductive AtCERK1 dimer by overexpression of AtCERK1-ECD compromises AtCERK1-mediated signaling in plant cells. Together, our data support the notion that chitin-induced AtCERK1 dimerization is critical for its activation.

In plants, pathogen-associated molecular pattern (PAMP)–induced immunity is mediated by the typically membrane-anchored proteins (*1*–*3*) pattern recognition receptors (PRRs), most of which are receptor-like kinases (RLKs) (*4*). Several PRRs (*5*–*9*) have been identified, including those critical for chitin-induced immune responses. Chitin, a polymer of *N*-acetyl-D-glucosamine (NAG), is a well-known PAMP that elicits plant immunity (*10*). The first chitin receptor identified in rice (*Oryza sativa*), OsCEBiP (*9*), carries an extracellular lysine motif (LysM) domain that is widely distributed for NAG recognition (*11*). In *Arabidopsis*, a CEBiP homolog, AtCERK1 (*5*) or LysM RLK1 (*6*), is required for chitin-triggered immunity. LysM-containing receptors appear to have a conserved role in chitin perception, as they also contributed to chitin-induced plant defenses in other species (*12*, *13*). AtCERK1 is also involved in detecting the bacteria-derived peptidoglycans (PGNs) to mediate *Arabidopsis* immunity (*14*, *15*). Besides plant defenses, LysM-containing proteins recognize the chitin-related molecules, Nod factors, to initiate root nodulation (*16*).

AtCERK1 has been established as a chitin receptor (*5*, *6*, *17*, *18*), and the AtCERK1-ECD containing three tandem LysMs (LysM1-3) directly recognizes chitin to signal plants for immunity (*17*, *18*). Chitin binding induces phosphorylation of the intracellular kinase domain of AtCERK1 (*17*) and activates disease resistance (*5*, *6*, *10*, *19*, *20*). Here we present biochemical, molecular, and structural data (table S1) supporting a model in which chitin-induced oligomerization is important for AtCERK1 activation, providing a template for understanding PAMP-induced PRR activation.

The three LysMs pack tightly against each other, resulting in a globular structure. Each LysM contains a βααβ structure in which the two β strands form an antiparallel β sheet (Fig. 1). The three LysMs share a conserved architecture (fig. S1A) that is similar to those of other LysM-containing proteins (fig. S2). The comparatively conserved residues among the three LysMs are limited to the βααβ regions (fig. S1B). Though making few contacts with each other, LysM2 and LysM3 pack tightly against LysM1. β1 in LysM1 and its counterpart β5 in LysM3 form a parallel β sheet, relating the two LysMs in a quasi two-symmetry axis (Fig. 1, left). LysM1 and LysM2 are also related by a quasi two-symmetry axis but through packing of different structural elements (Fig. 1, right). The tight packing of the three LysMs suggests that deletion of one LysM could

[1]Graduate Program in Chinese Academy of Medical Sciences and Peking Union Medical College, Beijing 100730, China. [2]Tsinghua-Peking Center for Life Sciences, Beijing 100084, China. [3]School of Life Sciences, Tsinghua University, Beijing 100084, China. [4]National Institute of Biological Sciences, No. 7 Science Park Road, Beijing 102206, China. [5]School of Life Science, Nanjing University, Nanjing 210093, China. [6]Department of Chemistry, Zhengzhou University, Zhengzhou 450001, China. [7]Beijing NMR Center, Peking University, Beijing 100871, China. [8]College of Life Sciences, Peking University, Beijing 100871, China. [9]State Key Laboratory of Plant Genomics and National Center for Plant Gene Research, Institute of Genetics and Developmental Biology, Chinese Academy of Sciences, Beijing 100101, China.

*These authors contributed equally to this work.
†To whom correspondence should be addressed: chaijj@mail.tsinghua.edu.cn (J.Chai); jmzhou@genetics.ac.cn (J.-M.Z.); changjunbiao@zzu.edu.cn (J.Chang)

generate a deleterious effect on the structural integrity of the other two.

The CXC motif harbored in the variable intervening sequences between the LyMs of AtCERK1 is conserved among the LysM-containing RLKs (*5*, *6*, *9*, *16*). Together with the N-terminal two cysteine (Cys) residues of LysM1, the four Cys residues from the two CXC motifs of AtCERK1 make three pairs of disulfide bridges (fig. S1B). Five potential glycosylation sites (fig. S3) defined by sufficient electron density (not shown) were found in the AtCERK1-ECD.

Despite the similarity of the three LysMs, only LysM2 was found to bind to $(NAG)_5$. However, it remains undetermined whether the other two LysMs are capable of binding to chitin. No conformational change occurs to AtCERK1-ECD after chitin binding (fig. S4). Electron density defines four of the five NAGs anchoring to a shallow groove that is created by two loops (L1 and L2) and lined with a few cavities at the bottom (Fig. 2A). A similar chitin-binding region was also found in another LysM-containing protein (*21*). The NAG units exhibit an alternation of ~180° flipping along the chain, adopting a fully extended conformation closely matching the surface topology of the groove (Fig. 2A).

The rings of NAG-2 and NAG-3 stack against L2, whereas no interaction exists between the remaining two rings and LysM2 (Fig. 2B). $(NAG)_5$-LysM2 interactions are established mainly through some of the branched groups from one side of $(NAG)_5$, providing numerous hydrogen bonds with the main chain of AtCERK1-ECD (Fig. 2B). Specific recognition of the *N*-acetyl moieties in NAGs allows AtCERK1 to distinguish chitin from glucose. In NAG-4, the carbonyl oxygen of the *N*-acetyl portion hydrogen bonds with the backbone-nitrogen of Glu^{114}, whereas the methyl group engages contacts with the side chains of Met^{127}, Gln^{131}, and Ala^{138}. A water molecule fills between NAG-4 and LsyM2, bridging a hydrogen bond between the C3 hydroxyl group and the main-chain nitrogen of Tyr^{113}. NAG-2 inserts its *N*-acetyl group deeply into a clear-cut pocket, allowing its carbonyl oxygen and amide nitrogen to hydrogen bond with the main-chain nitrogen

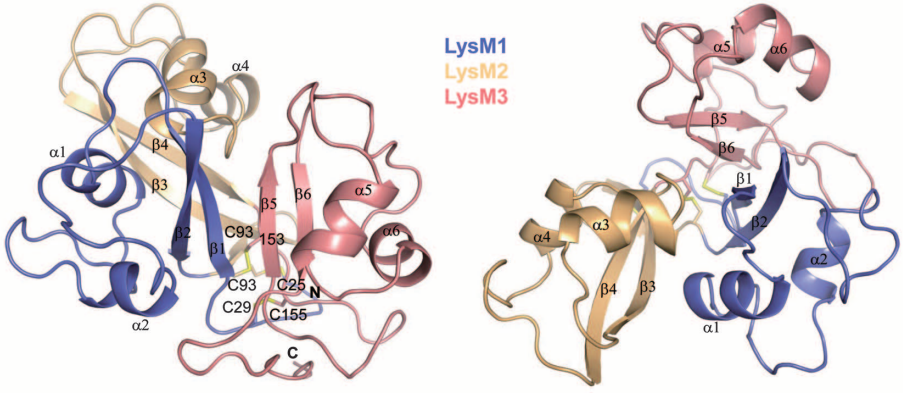

Fig. 1. Tight packing of the three LysMs in AtCERK1-ECD. Overall structures of AtCERK1-ECD in two different orientations. The secondary-structure elements are labeled. Disulfide bonds (C29-C155, C25-C93, and C93-C153) are labeled and shown in yellow stick.

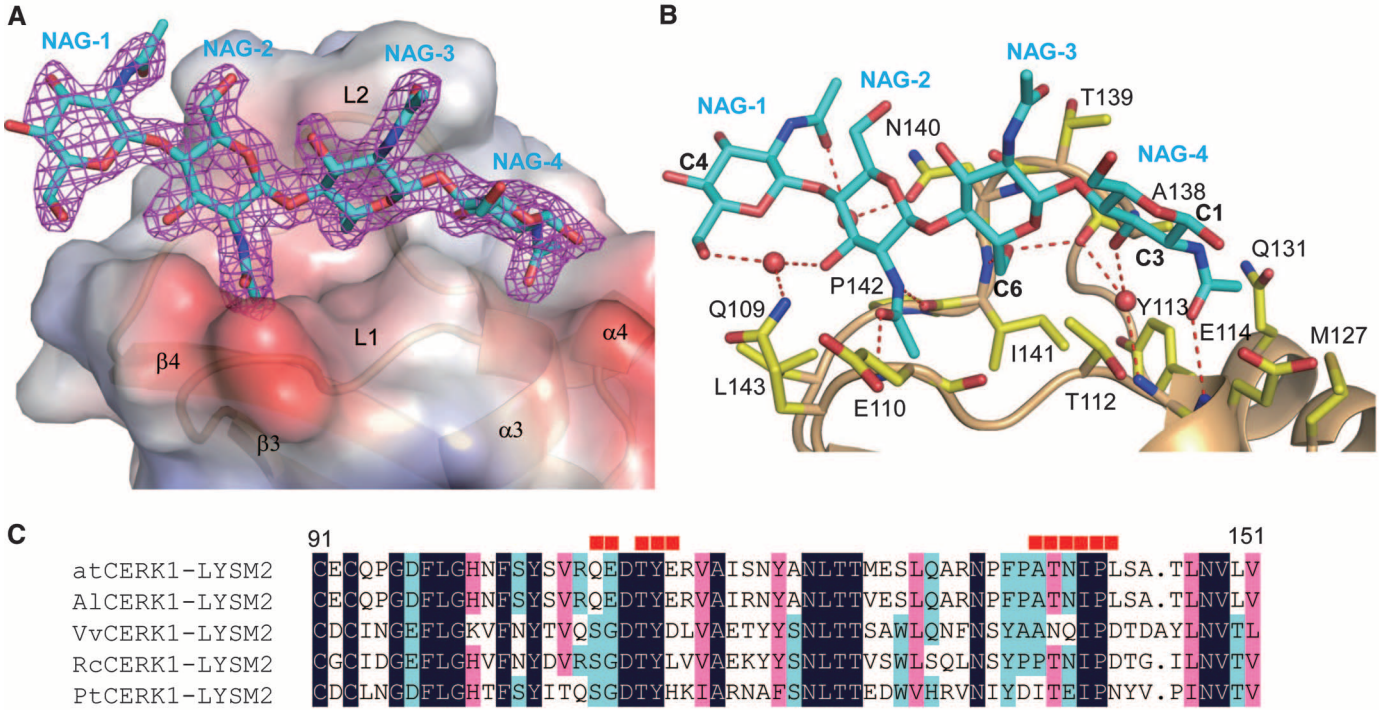

Fig. 2. Specific recognition of a chitin oligomer by AtCERK1-ECD. (**A**) Chitin binds to a shallow surface groove on AtCERK1-ECD. AtCEKR1-ECD is shown in electrostatic surface (transparency) and cartoon. White, blue, and red indicate neutral, positive, and negative surfaces, respectively. Shown in magenta mesh is the omit electron density ($F_o - F_c$, 2.8σ) around the bound chitin oligomer. Chitin residues are labeled (NAG1-4). (**B**) Detailed interactions between chitin and the AtCERK1-ECD. The side chains from AtCERK1 are shown in yellow. Red spheres represent oxygen atoms of water molecules. Four carbon atoms of the chitin oligomer are indicated (C1, C3, C4, and C6 in bold). The distance cut-off is 3.4 Å. (**C**) Sequence alignment of CERK1-LysM2 from different species. Red squares indicate the residues from LysM2 involved in interaction with chitin. At: *Arabidopsis thaliana*; Al: *Arabidopsis lyrata*; Vv: *Vitis vinifera*; Rc: *Ricinus communis*; Pt: *Populus trichocarpa*. Single-letter abbreviations for the amino acid residues are as follows: A, Ala; C, Cys; D, Asp; E, Glu; F, Phe; G, Gly; H, His; I, Ile; K, Lys; L, Leu; M, Met; N, Asn; P, Pro; Q, Gln; R, Arg; S, Ser; T, Thr; V, Val; W, Trp; and Y, Tyr.

of Glu[110] and the carbonyl oxygen of Ile[141], respectively (Fig. 2, A and B). NAG-3 is stabilized by van der Waals interactions between the hydroxymethyl group (C6) and its surrounding residues. Additionally, the C6 hydroxyl of NAG-3 participates in cooperative hydrogen bonds involving the backbone nitrogen of Ile[141] and carbonyl oxygen of Ala[138] (Fig. 2B). Interaction of NAG-1 with LysM2 is exclusively through water-mediated hydrogen bonds. The residues around the chitin-binding site of LysM2 are highly variable in the other two LysMs (fig. S1B) but comparatively conserved among different plants (Fig. 2C).

As both ends of the bound chitin fragment protrude out into the solvent region, extension of the chitin chain to either direction would not provide many additional, if any, chitin-LysM2 interactions. Consistently, different chitin oligomers exhibited small differences in AtCERK1-ECD–binding activity as quantified by isothermal titration calorimetry (fig. S5). However, biological activity varies considerably among different chitin fragments, with highest activity for heptamers and octamers (*22*), and little (*17*) or no activity (*23*) for tetramers and pentamers, though the latter two can bind to AtCERK1 (*17*, *18*). We hypothesized that higher oligomeric chitins like $(NAG)_8$ can simultaneously bind two or more AtCERK1 molecules and that the clustered AtCERK1 may be required for signaling.

To test the hypothesis, we examined the interaction between His_6- and hemagglutinin (HA)–tagged AtCERK1-ECD in the presence of different chitin oligomers or PGN using pull-down assay. In contrast with the shorter chitin oligomers and PGN, $(NAG)_8$ induced a strong interaction between the HA-tagged and His_6-tagged AtCERK1-ECDs (Fig. 3A). Supporting the observations, our nuclear magnetic resonance (NMR) (Fig. 3B and figs. S6 and S7) and gel filtration assays (fig. S8) showed that $(NAG)_8$ but not $(NAG)_4$ or $(NAG)_5$ induced AtCERK1-ECD dimerization in solution. Substitution of Ala[138] (Fig. 2B) with the bulkier histidine is expected to circumscribe the chitin-binding site and interfere with chitin binding. Indeed, the mutant protein A138H exhibited a weakened $(NAG)_5$-binding activity (fig. S5) and compromised $(NAG)_8$-induced dimerization in pull-down (Fig. 3A) and gel filtration (fig. S8) assays. Consistent with the in vitro data, chitin (Fig. 3C) or $(NAG)_8$ (fig. S9), but not PGN, induced dimerization of AtCERK1-FLAG and AtCERK1-HA proteins lacking the intracel-

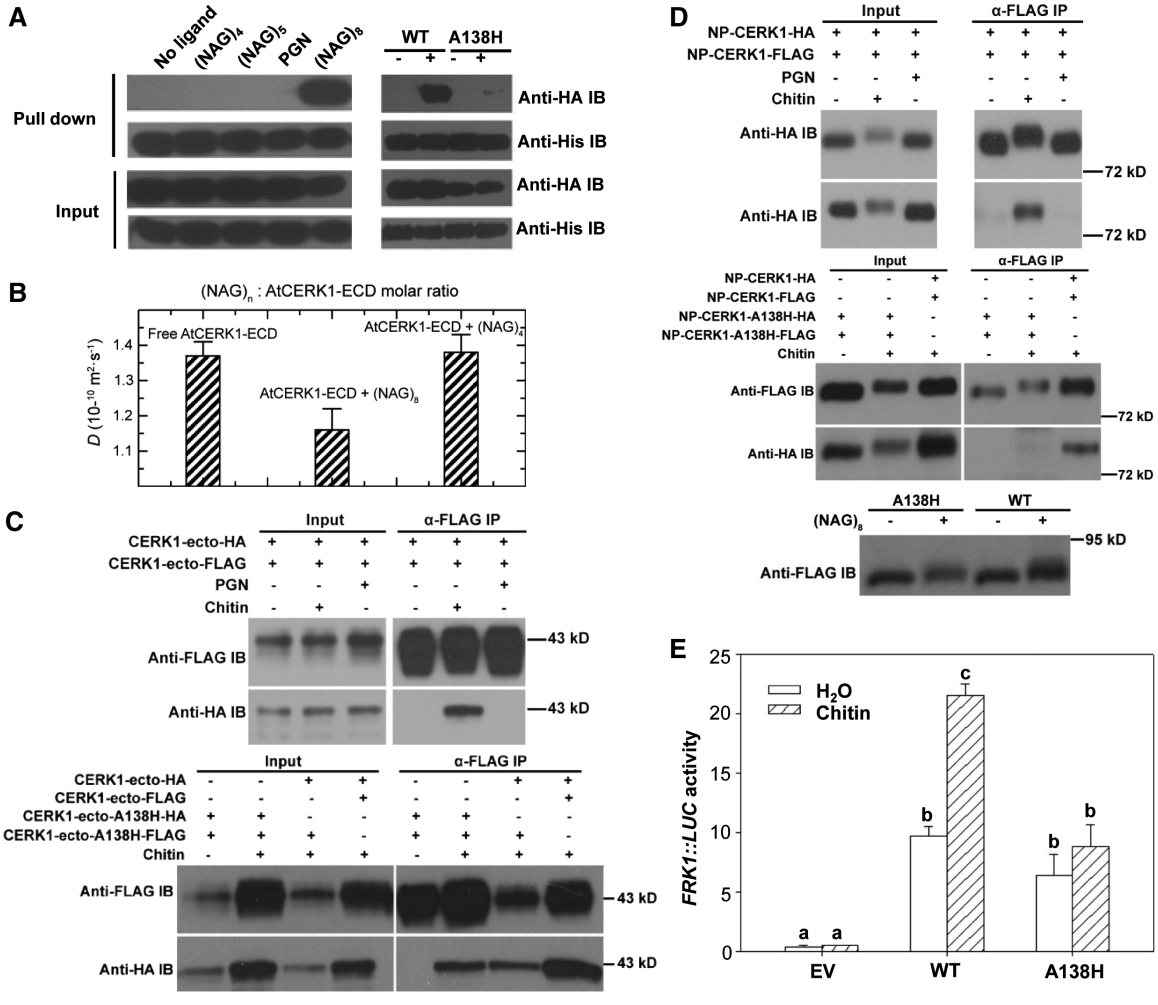

Fig. 3. Chitin-induced AtCERK1-ECD dimerization is critical for signaling. (**A**) Chitin octamer induces AtCERK1-ECD dimerization in vitro. An equal amount of His_6- and HA-tagged AtCERK1-ECD proteins were mixed and supplemented with different chitin oligomers, as indicated, and PGN. After incubation, the mixture was loaded onto Ni-resin and then washed extensively. The eluted proteins were detected by Western blot with antibodies against His and HA. (**B**) $(NAG)_8$ but not $(NAG)_4$ induces AtCERK1-ECD oligomerization in solution. The translational diffusion coefficients D of free AtCERK1-ECD, and in the presence of excess $(NAG)_n$, were determined by pulsed field gradient–NMR diffusion experiments. The molar ratio of $(NAG)_n$: AtCERK1-ECD was 2:1. (**C**) Chitin induces AtCERK1-ECD dimerization in protoplasts. Top: HA- and FLAG-tagged AtCERK1-ECDs were co-expressed in wild-type (WT) *Arabidopsis* protoplasts. Coimmunoprecipitation assay was performed to detect chitin-induced dimerization after treatment with (+) or without (–) chitin (200 μg/ml). Bottom: A138H substitution attenuates chitin-induced AtCERK1-ECD dimerization. (**D**) Chitin induces dimerization of the full-length AtCERK1 protein in protoplasts. Top: HA- and FLAG-tagged AtCERK1 were coexpressed in WT *Arabidopsis* protoplasts under the control of native AtCERK1 promoter. Methods described in (C) were used to detect the proteins. Middle: A138H substitution attenuates chitin-induced dimerization of the full-length AtCERK1 protein. NP: native promoter. Bottom: A138H substitution attenuates $(NAG)_8$-induced band shift of AtCERK1 protein in stable transgenic plants. Leaves of T1 transgenic plants were treated with H_2O or 60 μM $(NAG)_8$ for 15 min, and anti-FLAG immunoblot was used to detect band shift. (**E**) A138H attenuates chitin-induced *FRK1::LUC* expression. The *cerk1* mutant *Arabidopsis* protoplasts were transfected with empty vector (EV), AtCERK1 (WT), or AtCERK1-A138H (A138H) along with *35S::R-LUC* and *FRK1::LUC*. The *FRK1::LUC* activity was determined after protoplasts were treated with chitin (200 μg/ml) or H_2O for 3 hours. Different letters above the bars indicate significant difference (mean + SD; $n \geq 3$; $P < 0.01$).

lular kinase domain when coexpressed in protoplasts, which was reduced in the mutant protein A138H. Chitin-dependent dimerization was also observed for the wild-type AtCERK1 protein expressed under the control of native AtCERK1 promoter (NP-CERK1) but compromised in the mutant A138H protein (Fig. 3D). Notably, AtCERK1 overexpression resulted in chitin-independent AtCERK1 oligomerization and partial induction of *FRK1-LUC* (fig. S10), a reporter gene strongly induced by multiple PAMPs, including chitin (*1*). As previously reported (*17*), chitin induced a band shift of the AtCERK1 protein in protoplasts indicative of AtCERK1 phosphorylation, which surprisingly appeared not to be affected in the A138H mutant (Fig. 3D, middle). As demonstrated for flg22-induced FLS2 phosphorylation (*24*), ligand-induced phosphorylation of receptor kinases is a rapid process. Our protoplast-based assay may not be sensitive enough to distinguish the rapid phosphorylation in the wild-type AtCERK1 and the slow phosphorylation in the A138H mutant protein. Thus, although less effectively, the mutant protein was still fully phosphorylated at the time of detection. Consistently, $(NAG)_8$-induced AtCERK1 phosphorylation, which is less efficient than that by chitin (*17*), was reduced in stable transgenic plants expressing A138H (Fig. 3D, bottom). As previously reported (*5*), the *cerk1* mutant protoplasts were unable to activate *FRK1-LUC* transcription when induced with chitin (Fig. 3E). Introduction of the wild-type AtCERK1 but not the mutant A138H construct into the *cerk1* protoplasts led to increased *FRK1-LUC* expression, which was enhanced by chitin. Together, our data support the idea that chitin-induced cross-linking of AtCERK1 activates downstream signaling.

Given that $(NAG)_5$ bound to the AtCERK1-ECD but failed to induce its oligomerization, it was expected to interfere with $(NAG)_8$- or chitin-induced AtCERK1 oligomerization. As anticipated, $(NAG)_5$ attenuated $(NAG)_8$-induced AtCERK1-ECD dimerization in vitro in a dose-dependent manner (Fig. 4A). Similar results were obtained for AtCERK1-ECD expressed in protoplasts (Fig. 4B). Furthermore, $(NAG)_5$ reduced $(NAG)_8$-induced expression of *FRK1-LUC* in the wild-type protoplasts (Fig. 4C). We reasoned that if the chitin-induced AtCERK1 dimerization is required for signaling, overexpression of AtCERK1-ECD (OXLysM) would result in nonproductive dimerization and signaling blockage. Indeed, OXLysM led to its heterodimerization with full-length AtCERK1 in protoplasts and abolished chitin-induced expression of *FRK1-LUC* and band shift of AtCERK1 protein (Fig. 4C). $(NAG)_8$-induced accumulation of H_2O_2 in wild-type *Arabidopsis* plants was progressively reduced with increasing $(NAG)_5$ (Fig. 4D). Further supporting the dominant interactions of three NAGs with AtCERK1-ECD (Fig. 2B), the chemically synthesized compound Ch-2 with a linker connecting two $(NAG)_3$ (fig. S11) moderately induced AtCERK1-ECD dimerization in vitro (Fig. 4E), compared to a lower activity of Ch-1, and in protoplasts though less effectively than $(NAG)_8$ (Fig. 4F).

Our biochemical and molecular data show that $(NAG)_8$ can act as a bivalent ligand to induce cross-linking of AtCERK1-ECD required for chitin-induced signaling. The low chitin-binding activity of the isolated AtCERK1-ECD in solution may translate into tighter interactions in intact plant cells because in vivo the other part(s) of the full-length protein could stabilize the chitin-induced AtCERK1-ECD association. Additionally, anchoring to the two-dimensional lipid bilayer might limit diffusion of the AtCERK1 protein. Chitin-induced oligomerization was also found in the LysM-containing proteins ECP6 (*25*) and Hevein (*26*). A minimum length of chitin oligomers is expected for binding two AtCERK1-ECDs. It is unlikely that two AtCERK1-ECDs bind to $(NAG)_6$ with each peptide associating with three NAGs, as this would cause steric interactions between the two peptides. However, we cannot rule out the possibility that $(NAG)_6$ interacts with two AtCERK1-ECDs in an asymmetric mode, leading to weaker AtCERK1-ECD dimerization. Although $(NAG)_7$ and $(NAG)_8$ display the highest biological activity among the chitin oligomers tested, it remains unknown whether there exist longer chitin oligomers better optimized in length

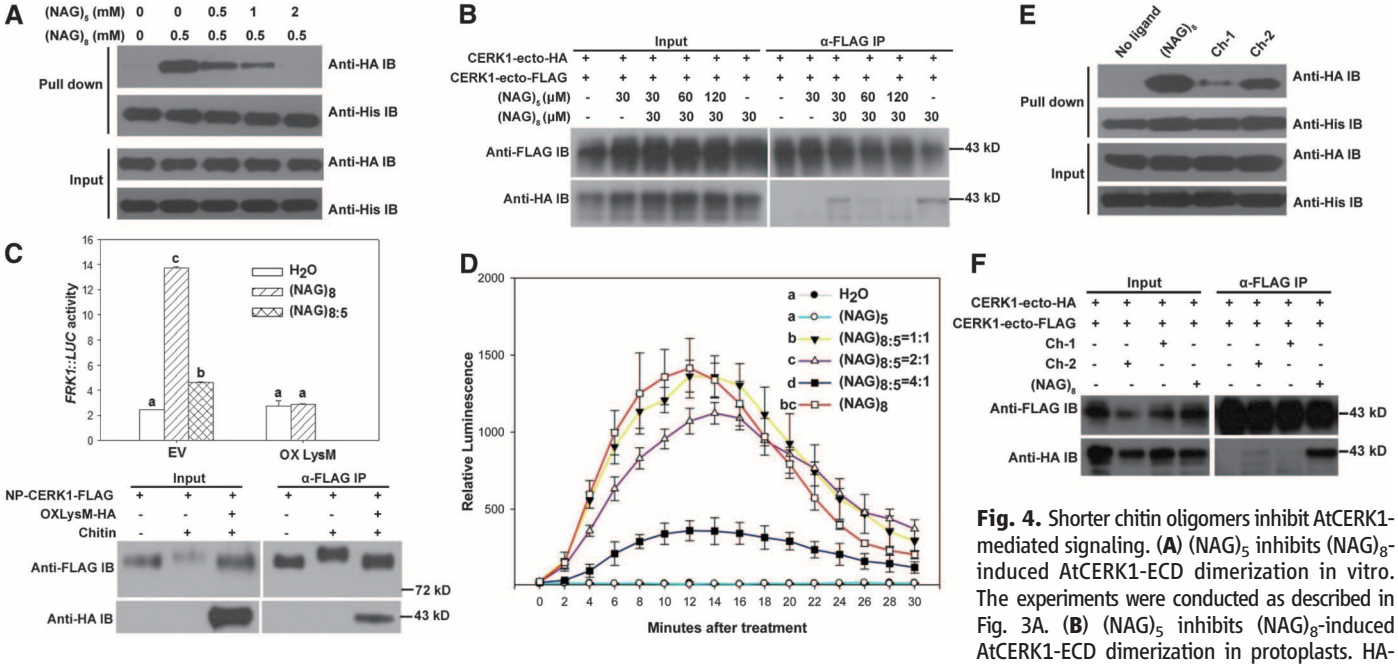

Fig. 4. Shorter chitin oligomers inhibit AtCERK1-mediated signaling. (**A**) $(NAG)_5$ inhibits $(NAG)_8$-induced AtCERK1-ECD dimerization in vitro. The experiments were conducted as described in Fig. 3A. (**B**) $(NAG)_5$ inhibits $(NAG)_8$-induced AtCERK1-ECD dimerization in protoplasts. HA- and FLAG-tagged AtCERK1-ECDs were coexpressed in WT *Arabidopsis* protoplasts, treated with H_2O (–) and chitin oligomers, as indicated, for 10 min, and coimmunoprecipitation assay was conducted to detect the dimerization. (**C**) $(NAG)_5$ and overexpression of AtCERK1-ECD (OXLysM) inhibit chitin-induced signaling. Top: Chitin induces heterodimerization between the overexpressed AtCERK1-ECD and the full-length AtCERK1. Bottom: OXLysM inhibits chitin-induced *FRK1::LUC* activity. WT *Arabidopsis* protopalsts were transfected with an empty vector (EV) or OXLysM plasmids along with *FRK1::LUC* and *35S::R-LUC*. The activity of *FRK1::LUC* was analyzed after treatment with 60 μM $(NAG)_8$ or a mixture of 60 μM $(NAG)_8$ and 240 μM $(NAG)_5$ [$(NAG)_{8:5}$] for 3 hours. Different letters above the bars indicate significant difference (mean + SD; $n \geq 3$ replicates; $P < 0.01$). (**D**) $(NAG)_5$ inhibits $(NAG)_8$-induced H_2O_2 production in planta. WT *Arabidopsis* leaves were treated with 30 μM $(NAG)_8$ or a mixture of 30 μM $(NAG)_8$ and $(NAG)_5$ with different ratios [$(NAG)_{8:5}$] as indicated (mean ± SD; $n \geq 4$; $P < 0.01$). (**E**) A synthetic chitin derivative induces AtCERK1-ECD dimerization in vitro. The experiments were performed as described in Fig. 3A. (**F**) AtCERK1-ECD dimerization in protoplasts in response to synthetic chitin derivatives. The experiments were performed as described in Fig. 3C.

and rigidity to allow more efficient AtCERK1 activation. The free hydroxyl groups at C4 and C1 (Fig. 2B) from the two ends of $(NAG)_4$ are not involved in AtCERK1-ECD binding, suggesting that chitin oligomers with more than eight units can interact with more than two AtCERK1 molecules simultaneously. Consistently, AtCERK1 interacts strongly with polymeric chitin (*17*) because of multiple AtCERK1-binding sites.

Like the mammalian receptor tyrosine kinases (RTKs) and toll-like receptors (TLRs), plant RLKs have emerged as critical regulators of key cellular processes. Structural analyses have demonstrated that ligand-induced dimerization is a common theme for the activation of RTKs (*27*) and TLRs (*28*). The molecular mechanisms underlying RLK activation, however, remain much less understood. Ligand-induced heterodimerization has been reported for several RLKs (*29*–*32*). Our results suggest that chitin-mediated cross-linking of AtCERK1s is required for immune signaling, shedding light on a molecular mechanism of ligand-induced RLK activation.

References and Notes

1. T. Boller, G. Felix, *Annu. Rev. Plant Biol.* **60**, 379 (2009).
2. C. Zipfel, *Curr. Opin. Immunol.* **20**, 10 (2008).
3. J. E. Parker, *Trends Plant Sci.* **8**, 245 (2003).
4. S. H. Shiu *et al.*, *Plant Cell* **16**, 1220 (2004).
5. A. Miya *et al.*, *Proc. Natl. Acad. Sci. U.S.A.* **104**, 19613 (2007).
6. J. Wan *et al.*, *Plant Cell* **20**, 471 (2008).
7. C. Zipfel *et al.*, *Cell* **125**, 749 (2006).
8. C. Zipfel *et al.*, *Nature* **428**, 764 (2004).
9. H. Kaku *et al.*, *Proc. Natl. Acad. Sci. U.S.A.* **103**, 11086 (2006).
10. T. Boller, *Annu. Rev. Plant. Physiol. Mol. Biol.* **46**, 189 (1995).
11. G. Buist, A. Steen, J. Kok, O. P. Kuipers, *Mol. Microbiol.* **68**, 838 (2008).
12. S. Tanaka *et al.*, *BMC Plant Biol.* **10**, 288 (2010).
13. J. Fliegmann *et al.*, *Plant Physiol. Biochem.* **49**, 709 (2011).
14. R. Willmann *et al.*, *Proc. Natl. Acad. Sci. U.S.A.* **108**, 19824 (2011).
15. S. Gimenez-Ibanez *et al.*, *Curr. Biol.* **19**, 423 (2009).
16. S. Radutoiu *et al.*, *Nature* **425**, 585 (2003).
17. E. K. Petutschnig, A. M. Jones, L. Serazetdinova, U. Lipka, V. Lipka, *J. Biol. Chem.* **285**, 28902 (2010).
18. E. Iizasa, M. Mitsutomi, Y. Nagano, *J. Biol. Chem.* **285**, 2996 (2010).
19. K. M. Ramonell *et al.*, *Mol. Plant Pathol.* **3**, 301 (2002).
20. N. Shibuya, E. Minami, *Physiol. Mol. Plant Pathol.* **59**, 223 (2001).
21. T. Ohnuma, S. Onaga, K. Murata, T. Taira, E. Katoh, *J. Biol. Chem.* **283**, 5178 (2008).
22. L. P. Hamel, N. Beaudoin, *Planta* **232**, 787 (2010).
23. B. Zhang, K. Ramonell, S. Somerville, G. Stacey, *Mol. Plant Microbe Interact.* **15**, 963 (2002).
24. B. Schulze *et al.*, *J. Biol. Chem.* **285**, 9444 (2010).
25. R. de Jonge *et al.*, *Science* **329**, 953 (2010).
26. J. L. Asensio *et al.*, *Chem. Biol.* **7**, 529 (2000).
27. M. A. Lemmon, J. Schlessinger, *Cell* **141**, 1117 (2010).
28. J. Y. Kang, J. O. Lee, *Annu. Rev. Biochem.* **80**, 917 (2011).
29. D. Chinchilla *et al.*, *Nature* **448**, 497 (2007).
30. A. Heese *et al.*, *Proc. Natl. Acad. Sci. U.S.A.* **104**, 12217 (2007).
31. J. Li *et al.*, *Cell* **110**, 213 (2002).
32. K. H. Nam, J. Li, *Cell* **110**, 203 (2002).

Acknowledgments: We thank F. Yu and J. He at Shanghai Synchrotron Radiation Facility (SSRF). J.C. was funded by State Key Program of National Natural Science of China (31130063) and Chinese Ministry of Science and Technology (2010CB835300). J.M.Z. was funded by Chinese Ministry of Science and Technology (2011CB100700; 2010CB835300). J.B.C. was funded by the National Outstanding Young Scholar Science Foundation of National Natural Science Foundation of China (30825043). The coordinates and structural factors for free- and chitin-bound AtCERK1-ECD have been deposited in Protein Data Bank with accession codes 4EBY and 4EBZ, respectively.

Supplementary Materials

www.sciencemag.org/cgi/content/full/336/6085/1160/DC1
Materials and Methods
Table S1
Figs. S1 to S11
References (*33*–*40*)

9 January 2012; accepted 23 April 2012
10.1126/science.1218867

Rocket Launcher Mechanism of Collaborative Actin Assembly Defined by Single-Molecule Imaging

Dennis Breitsprecher,[1] Richa Jaiswal,[1] Jeffrey P. Bombardier,[2] Christopher J. Gould,[1] Jeff Gelles,[2]* Bruce L. Goode[1]*

Interacting sets of actin assembly factors work together in cells, but the underlying mechanisms have remained obscure. We used triple-color single-molecule fluorescence microscopy to image the tumor suppressor adenomatous polyposis coli (APC) and the formin mDia1 during filament assembly. Complexes consisting of APC, mDia1, and actin monomers initiated actin filament formation, overcoming inhibition by capping protein and profilin. Upon filament polymerization, the complexes separated, with mDia1 moving processively on growing barbed ends while APC remained at the site of nucleation. Thus, the two assembly factors directly interact to initiate filament assembly and then separate but retain independent associations with either end of the growing filament.

Regulation of actin assembly is a fundamental requirement in all eukaryotic cells, and a growing number of factors have been identified that either inhibit or promote this process. For example, the combined presence of the actin monomer–binding protein profilin and the filament end–binding capping protein (CapZ) strongly suppresses both spontaneous filament nucleation and elongation. Thus, filament assembly in vivo requires nucleation and elongation factors to overcome these barriers to assembly (*1*–*3*). The formation of most cellular actin structures depends on two or more such factors, which often interact directly. A formin is a component of many actin assembly–promoting factor (APF) pairs that likely function together in vivo: the formins FMN/Cappucino (Capu) and Spire (*4*), the formin Bni1 and Bud6 (*5*), the formin mDia1 and adenomatous polyposis coli (APC) (*6*), and the formin dDia2 and *Dictyostelium* vasodilator-stimulated phosphoprotein (DdVASP) (*7*).

The dimeric formin–homology 2 (FH2) domain of formins processively tracks the growing barbed end of the actin filament, protecting it from capping proteins (*8*–*10*). Adjacent FH1 domains recruit profilin-actin complexes and can increase the rate of elongation at barbed ends (*11*). Whereas profilin enhances formin-mediated filament elongation, its presence also strongly suppresses filament nucleation by formins (*12*). Collaboration of formins with other APFs that bind multiple actin monomers (*4*–*6*, *13*) may be required to overcome the inhibitory effects of profilin and capping protein. However, direct evidence for this hypothesis has been lacking. To address this, we reconstituted mDia1-APC–mediated actin assembly with purified, fluorescently tagged proteins and used multiwavelength single-molecule TIRFM (total internal reflection fluorescence microscopy) to directly visualize and define the mechanisms promoting collaborative filament assembly.

For single-molecule imaging, we purified a soluble, modified O^6-alkylguanine-DNA alkyltransferase (AGT)-tagged (also known as SNAP–tag) C-terminal fragment of APC (APC-C): residues 2130–2843, encompassing its "Basic" domain, which is sufficient to mediate actin nucleation, and the domain that binds EB1 (a microtubule end–binding protein) (*6*, *14*). SNAP–APC-C labeled with SNAP-surface-647 (herein named SNAP-647-APC-C) displayed activities identical to those of APC-C in pyrene-actin assembly assays (fig. S1A). Photobleaching data suggested that most SNAP-647-APC-C molecules are dimeric (fig. S1, B and C; and movie S1), consistent with hydrodynamic studies on maltose-binding protein–tagged APC-C (*6*).

APC, like Spire and Bud6, has been proposed to catalyze actin nucleation by binding actin monomers to form an F-actin seed (*4*–*6*). We used dual-color TIRFM to directly visualize surface-adsorbed SNAP-647-APC-C molecules, appearing as discrete spots, during the assembly

[1]Department of Biology, Brandeis University, Waltham, MA 02454, USA. [2]Department of Biochemistry, Brandeis University, Waltham, MA 02454, USA.

*To whom correspondence should be addressed. E-mail: goode@brandeis.edu (B.L.G.); gelles@brandeis.edu (J.G.)

Chitin-Induced Dimerization Activates a Plant Immune Receptor

Tingting Liu, Zixu Liu, Chuanjun Song, Yunfei Hu, Zhifu Han, Ji She, Fangfang Fan, Jiawei Wang, Changwen Jin, Junbiao Chang, Jian-Min Zhou and Jijie Chai

Science **336** (6085), 1160-1164.
DOI: 10.1126/science.1218867

Dissecting Chitin Binding

The chitin in fungal cells walls serves as a trigger to initiate plant defenses against pathogenic fungi. *Arabidopsis* detects these signals through a cell surface chitin receptor whose intracellular kinase domain initiates a signaling cascade in response to chitin that activates the plant's response to infection. **Liu *et al.*** (p. 1160) have now solved the crystal structure of the *Arabidopsis* chitin receptor AtCERK1. The results show how chitin binds to the receptor and suggest that the biological response requires dimerisation of the receptor when it binds a chitin oligomer at least seven or eight subunits long.